a single Compton camera. Thus, multiple molecular imaging is a natural application of GREI.

In this work, we tried to demonstrate the concept of multiple molecular imaging with semiconductor Compton cameras, by showing simultaneous imaging of different γ-ray emitting radionuclides in wide energy range. Three radioactive tracers were simultaneously injected to a live mouse, including a SPECT imaging agent that can visualize some biological functions, and simultaneous imaging of the tracers was performed by using a prototype of a GREI apparatus.

Demonstration of multiple molecular imaging in live mouse

The experimental animal was a male normal ICR mouse at 8 weeks of age. Three radioactive tracers were intravenously injected to the mouse by the following procedures: (1) iodinated (^{131}I) methylnorcholostenol (18.5 MBq) was injected by dividing into three doses, injected 5-, 4- and 3-days prior to the imaging. To allow dissociated ^{131}I to be uptaken to the thyroid gland, no thyroid blocking agent was used. (2) $^{85}SrCl_2$–saline (2.0 MBq) was injected 1 day prior to the imaging. (3) $^{65}ZnCl_2$–saline (2.0 MBq) was injected 25 minutes prior to the imaging. The mouse was bound to the imaging stage equipped with a worming pad. The imager was installed front face down right above the imaging stage. The distance between the stage surface and the front detector of the GREI apparatus was 45 mm. The imaging was carried out for 12 hours, with the mouse treated under Nembutal anesthesia. The acquired data were analyzed on-line for checking, and also recorded in list-mode with real time and live time information for further off-line analysis. The experiment had been approved by Wako Animal Experiment Committee of RIKEN, and was performed in compliance with Regulations for the Animal Experiments of RIKEN and related laws.

Results and discussion

Two-dimensional (2D), and three dimensional (3D) images were reconstructed from the data acquired from the live-mouse imaging experiment, by adopting the image-reconstruction methods described in ref. 2. For the 2D images, a horizontal (coronal) plane at 34 mm from the front detector was chosen, which intersects the approximate center of the mouse body.

Fig. 2 shows the γ-ray energy spectrum constructed from the acquired data. Image reconstruction was carried out for each tracer by setting ±5 keV energy windows around each specific γ-ray photopeak.

The *in vivo* behavior of the tracers used in this work has been well studied.[3–6] ^{65}Zn accumulates in the liver and the tumor; ^{85}Sr is a bone seeking nuclide; and iodinated (^{131}I) methylnorcholostenol accumulates in the adrenal glands, and dissociated ^{131}I accumulates in the thyroid gland if no thyroid blocking agent is used.

Fig. 3 shows the results of the 2D image reconstruction. As mentioned in ref. 2, the 2D images do not represent true tomographic slices because they ignore the tracer distribution outside

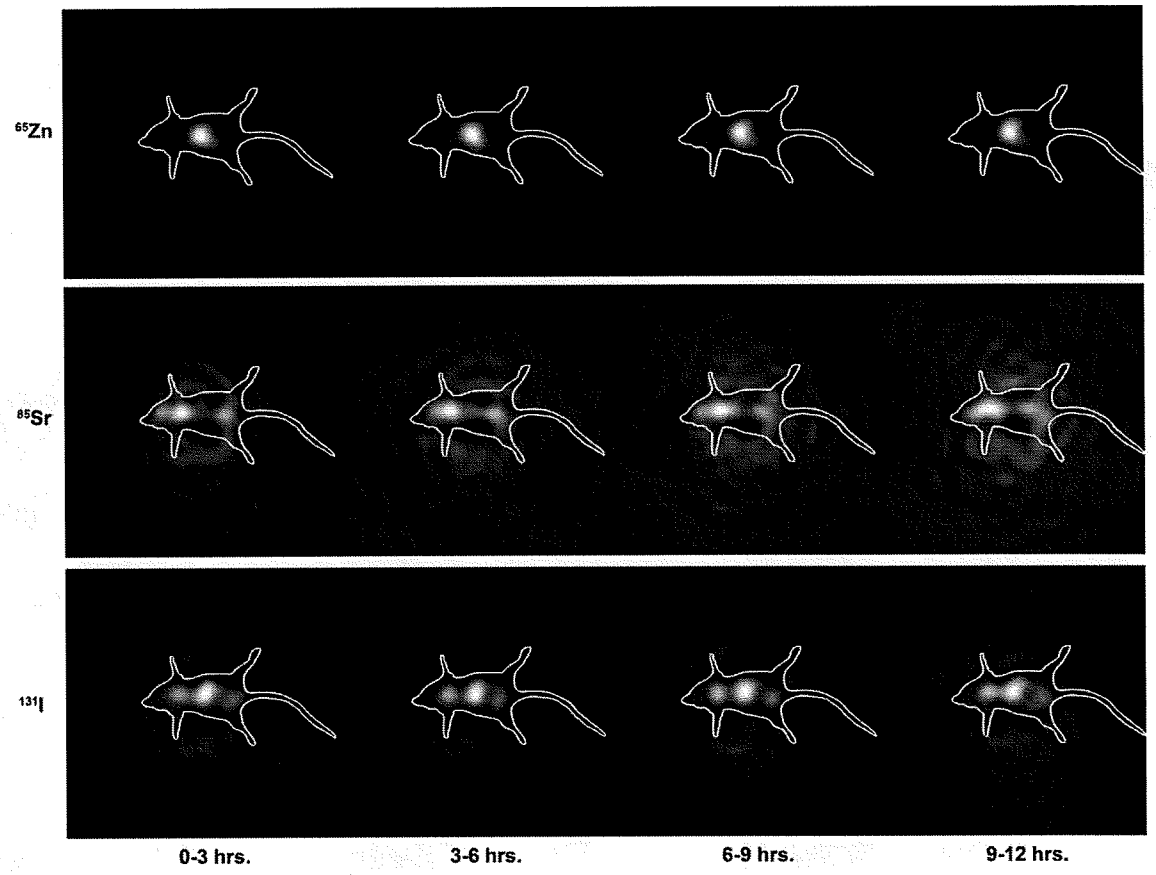

Fig. 5 Sequential images of each tracer, reconstructed for each time span.

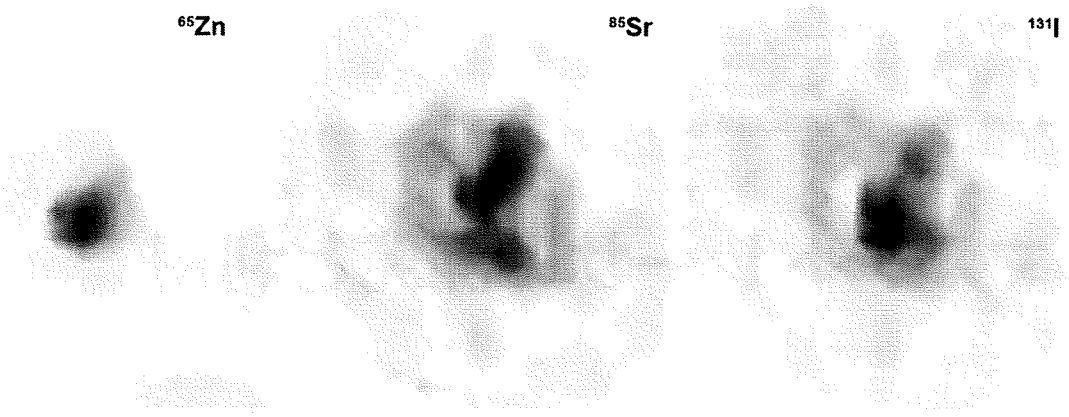

Fig. 6 Maximum intensity projection images of 3D reconstructed images for ^{65}Zn, ^{85}Sr and ^{131}I.

the 2D plane. However, the 2D images have apparently represented the characteristic behavior of each tracer, that is: ^{65}Zn accumulated in the liver; ^{85}Sr accumulated along bones; and ^{131}I accumulated in the adrenal glands, and dissociated ^{131}I accumulated in the thyroid gland.

Fig. 4 shows some examples of representing the 2D images. The image intensities of ^{65}Zn, ^{131}I and ^{85}Sr were assigned red, green and blue colored pixels, respectively, and overlaid with the photograph of the mouse. By using this method, any two or three tracers could be displayed in one picture.

Fig. 5 shows the sequential images of each tracer that could show the dynamic metabolic processes, constructed for each time span of 0 to 3, 3 to 6, 6 to 9 and 9 to 12 h. The time spans are variable by changing the sectioning of the list-mode data. In the figures, little significant change of tracer distribution was observed, showing the equilibrium state of the tracer concentration during the imaging time.

In order to obtain true tomographic images, 3D image reconstruction was performed. Fig. 6 shows the maximum intensity projection images of the 3D reconstructed images in tilted view, though they are still preliminary results. However, the different distribution suggests that the characteristic behavior of each tracer was represented in the figures, and the 3D distribution was able to be reconstructed.

As shown above, we were able to obtain quite encouraging results for multiple molecular imaging by use of semiconductor Compton cameras. However, a higher spatial resolution, a shorter imaging time, and quantitation would be required for more practical use. Our preliminary estimation has shown that a spatial resolution of less than 1 mm and about ten times improved detection efficiency could be achieved. And also importantly, targeted molecular events and efficacious molecular probes must be developed to extract full potential of multiple molecular imaging with GREI. Though the cost is one of the major problems for germanium semiconductor detectors, whether it is expensive or not depends on the importance of the targeted molecular events. We are pursuing research and development on these requirements, and we believe that they will be met in the not too distant future.

Conclusions

We demonstrated the concept of multiple molecular imaging by use of semiconductor Compton cameras. The GREI apparatus, which is a Compton camera consisting of two double-sided orthogonal-strip Ge detectors, was used for the γ-ray imaging. Three radioactive tracers of $^{65}ZnCl_2$, $^{85}SrCl_2$, and iodinated (^{131}I) methylnorcholestenol were simultaneously administered to a mouse, and the γ-ray imaging was carried out for 12 hours with the mouse treated under anesthesia. We were able to obtain 2D and 3D images of the tracers simultaneously, which showed the potential of GREI apparatus as a multiple molecular imager. We are pursuing research and development to realize the full potential of multiple molecular imaging with semiconductor Compton cameras.

Acknowledgements

This research was supported by Molecular Imaging Research Program of Japan's Ministry of Education, Culture, Sports, Science and Technology, Grants-in-aid for Scientific Research of Japan's Ministry of Health, Labor and Welfare, and R&D project of Molecule Imaging Equipment for Malignant Tumor Therapy Support of New Energy and Industrial Technology Development Organization.

References

1 H. Haba, D. Kaji, Y. Kanayama, K. Igarashi and S. Enomoto, *Radiochim. Acta*, 2005, **93**, 539–542.
2 S. Motomura, S. Enomoto, H. Haba, K. Igarashi, Y. Gono and Y. Yano, *IEEE Trans. Nucl. Sci.*, 2007, **54**, 710.
3 *Heavy Metals in the Environment*, ed. B. Sarkar, Marcel Dekker Inc., New York, USA, 2002.
4 C. Reilly, *The Nutritional Trace Metals*, Blackwell Publishing Ltd, Oxford, UK, 2004.
5 S. Enomoto, *Biomed. Res. Trace Elem.*, 2005, **16**, 233.
6 M. Kojima, M. Maeda, H. Ogawa, K. Nitta and T. Ito, *J. Nucl. Med.*, 1975, **16**, 666.

展望 TENBO

マルチトレーサの開発と利用

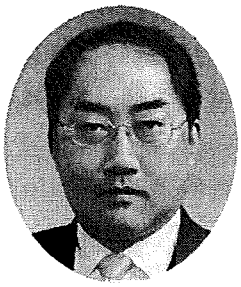
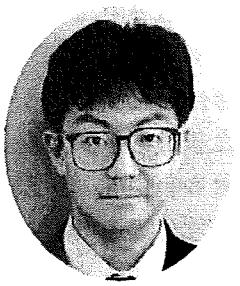

榎本　秀一　*Enomoto Shuichi*
羽場　宏光　*Haba Hiromitsu*
（独立行政法人理化学研究所）

1 はじめに

放射性同位元素（RI）を利用した研究は，広範な分野において応用研究が展開され，基礎から臨床応用まで含めて多くの成果が報告されている。生体における必須微量元素や環境中から曝露される様々な元素に関する研究において，RIの有用性は言及する必要もないであろう。我が国におけるトレーサ技術の利用は，1950年代ころから始まり，医学，薬学，生物学，農学，栄養学，環境科学などの広範な応用研究に用いるようになってきた。これらの研究は，RIを使用しない他の手法に比べて，極めて感度が高い点が特筆すべきことである。RIトレーサ法は担体を含まないか，極微量のRIと同じ元素の安定同位体を含んでいる。また，RIを用いてラベルした化合物を用いて研究する場合もラベルしていない物質や化合物と化学的にもほぼ同等であり，代謝バランスや生理的状態に影響をほとんど与えることなく，ダイナミクスを反映している。

本稿では生体微量元素研究を始めとするさまざまな研究のツールとして用いられているマルチトレーサ法（多元素同時代謝追跡法）の開発と最近の利用研究に触れたい。

2 マルチトレーサ法

マルチトレーサ法は，1991年に理化学研究所（理研）の安部文敏主任研究員らによって考案された[1]。これは理研の加速器施設（現 仁科加速器研究センター）のリングサイクロトロンで加速される重イオンの多様性とそのエネルギー領域での核反応の特徴を生かし，多数の元素についてその化学的，生物学的挙動の同時追跡を可能にする新しいトレーサ技術であり，マルチトレーサ法と命名された。1994年に著者らは，動物における微量元素研究にマルチトレーサ法が有効であることを予測し，微量元素の生体内挙動に関する知見と従来の研究成果の比較をすることから研究をスタートした。現在まで生物，医学，化学，環境科学など多くの研究分野でマルチトレーサ法を用いた応用研究がなされている。詳細は著者の総説などを参照いただ

きたい[2]。

1991年から2003年まで安部らの作成した落送管式マルチトレーサ製造装置が稼動してきたが，マルチトレーサのユーザー増加と効率的製造法の確立を目指し，2003年後半より，照射システムの抜本的改良を行い，これによって製造技術は高度化され，高効率化と製造のオンライン化も行われた[3]。現在，理研の加速器施設に設置されているマルチトレーサ製造ラインの模式図を図1に装置の写真を図2に示す。近年，京都大学の柴田誠一らは，原子炉を利用した核分裂生成物を用いたFissionマルチトレーサも実用化し，環境科学分野の応用研究が推進されている[4]。

マルチトレーサ法は，同時に製造した多数の元素のRIを用いることにより，多数の元素についてその物理的，化学的，生物学的挙動の同時追跡を可能にするトレーサ技術である。RIトレーサは，これまで単独で，あるいは，ごく少数のトレーサを組み合わせて使われてきた。しかし，半導体検出器とコンピュータの普及で，γ線放出核については，多数のRIからのγ線を同時に測定し，データ処理によって個々のRIを定量することが容易になった。RIはそれぞれ固有のエネルギーのγ線（多くの場合複数）を放出するが，高純度Ge半導体検出器を使うと，これらのγ線スペクトルを高分解能で測定できる。多数のRIが共存する場合，スペクトル線の一部は重なり合うが，既存のプログラムで解析することができる。実際，原子炉を用いた機器中性子放射化分析法ではこの技術が一般に使われている。

理研リングサイクロトロンはTaまでのイオンを加速する性能を持つ重イオン加速器で，C，N，Oなどのイオンは核子（原子核中の陽子と中性子）1個当たり135 MeVにまで加速することができる。このような高エネルギーの重イオンで照射を行うと，ターゲット中の原子核と加速されたイオンの核の接触した部分が互いに破砕される核破砕反応（Nuclear Fragmentation Reaction）が起きる。そして，両方の核の残った部分は，多くの場合不安定核となる。このとき，ターゲット核と加速イオンの核の接触の仕方は様々なので，多様な放射性核種が生成し，

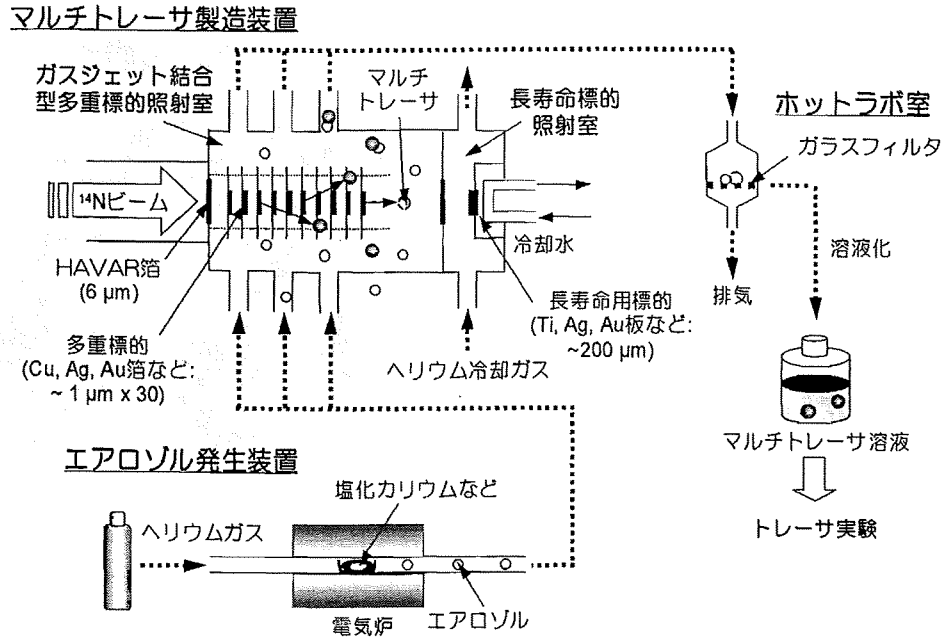

図1　理研リングサイクロトロンによるマルチトレーサの製造，
ガスジェット結合型多重ターゲット照射システムの概略図

その多くはγ線放出体である。この核反応を利用してマルチトレーサを製造する。ターゲットとしては，Au，Ag，Tiなどを繁用しており，ターゲット中にはターゲット物質に応じて，多数の元素のRIが生成するので，その中のγ線放出体を利用する。一般には，ターゲットより原子番号の少ないすべての元素の原子核ができる。これまでに製造されたマルチトレーサにγ線放出体が含まれる元素を図3の周期表上に示した。Tl以上の元素については現在，利用者がほとんどないので，製造技術開発は行っていない。Sb以下で白抜きのままに残っているのは主として適当な半減期のγ線放出体のない元素である。重イオンの照射後，ターゲットを酸に溶解し，担体であるターゲット物質を化学的に除去すれば，多数の元素のRIを含むマルチトレーサ溶液が得られる。これらのRIは，いわゆる無担体の状態，すなわち各RIの安定同位体をほとんど含まない状態で得られる。また，化学分離操作を工夫することで，分離操作に由来する塩（例えばNaCl）を含まない状態で得ることもできる。このようにして得られたマルチトレーサは，そのまま，あるいは必要に応じてさらに群分離を行ってグループトレーサとし，種々の系について多数の元素の物理的，化学的，生物学的挙動の同時追跡に用いる。マルチトレーサ中に含まれる多数のRIの個々の定量は，試料のγ線スペクトルを高純度Ge半導体検出器で測定し，得られるスペクトルを計算機処理して行う。昨今は，マルチトレーサでスクリーニングして，めぼしをつけた興味深い振る舞いの元素をAVFサイクロトロンでシングルトレーサとして製造し，それを用いて詳細な研究が進められるケースも多い。また，最

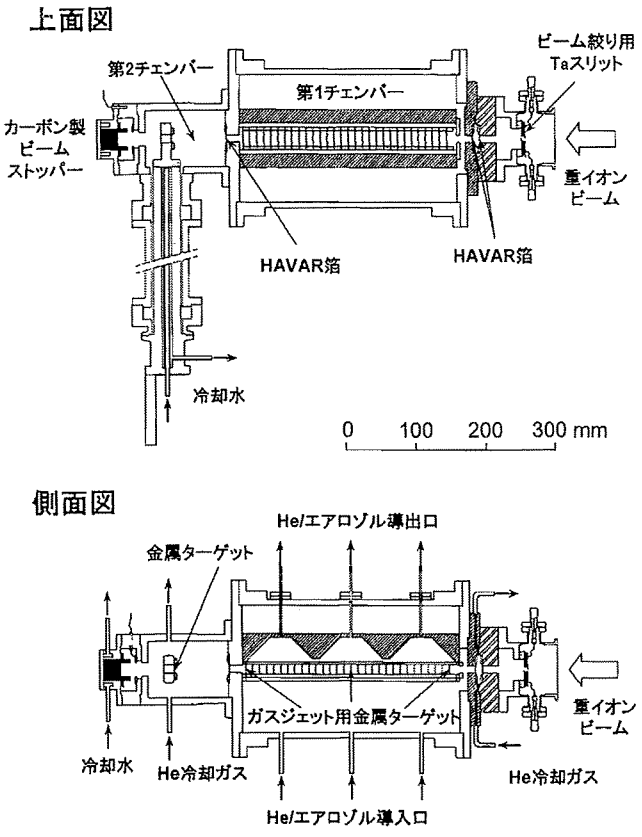

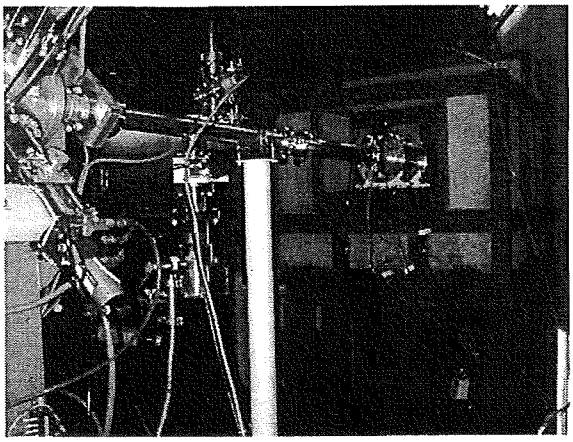

図2　理研リングサイクロトロンによるマルチトレーサの製造，ガスジェット結合型多重ターゲット照射システムの写真

近，著者らの開発しているコンプトンカメラ方式による複数分子同時ガンマ線イメージング装置 GREI（γ-ray Emission Imaging）は，マルチトレーサのような複数核種の同時非破壊イメージングにも応用できるので，その装置の開発は，新しい分子イメージング装置としてのみならず，マルチトレーサの研究にとっても有用となることが期待されている[5,6]。

3 現在稼動しているマルチトレーサ製造ラインによるマルチトレーサ製造

理研リングサイクロトロンによって核子当たり 135 MeV まで加速した ^{14}N ビームを通常，銀板や金板などの標的に照射し，図 1，2 に示した装置でマルチトレーサを製造している。本装置の特徴は，比較的短寿命の RI 製造を目的としたガスジェット結合型多重標的照射室（新システム）と長寿命 RI の製造（従来のマルチトレーサと同じ）を目的とした照射室に分かれていることである。高真空（$\sim 10^{-6}$ Pa）のビームラインとヘリウムガス（~100 kPa）で満たされた 2 つの照射室の間は，それぞれ厚さ 6 μm の HAVAR 箔で仕切られている。^{14}N ビームは，まず 10 mm の間隔を空けてスタックされた厚さ数 μm の標的を 30 枚貫く。エアロゾル発生装置で生成した塩化カリウムのエアロゾルは，ヘリウムガスをキャリアーとして照射室に導入される。核反応で標的から反跳分離されたマルチトレーサは，ヘリウムガス中で減速され，エアロゾルに吸着され，ガスジェットによって数秒のうちに地下のホットラボ室へ輸送される。ホットラボ室では，マルチトレーサを吸着したエアロゾルはガラスフィルタに捕集され，これを任意の溶液に溶解することによって直ちに応用研究可能なマルチトレーサ溶液が得られる。この方法では標的からの RI の化学分離が不要で，数秒程度の短寿命の RI までを研究の対象とできる特徴がある。周期表上のあらゆる元素を標的とでき，標的のスタック構成をアレンジすることでマルチトレーサに含まれる核種の種類や数量を最適化できる。さらに，ガスジェットを自動化学分離装置と結合すれば，特定の RI をイオン交換法や溶媒抽出法により濃縮分離でき，ユーザーの研究対象となる RI のみを含んだマルチトレーサも製造できる。本装置の性能試験として，著者らは，厚さ 2 μm の銅標的を 30 枚用いてマルチトレーサ製造実験を行った[3]。半減期 1 分以上の核種を対象に製造実

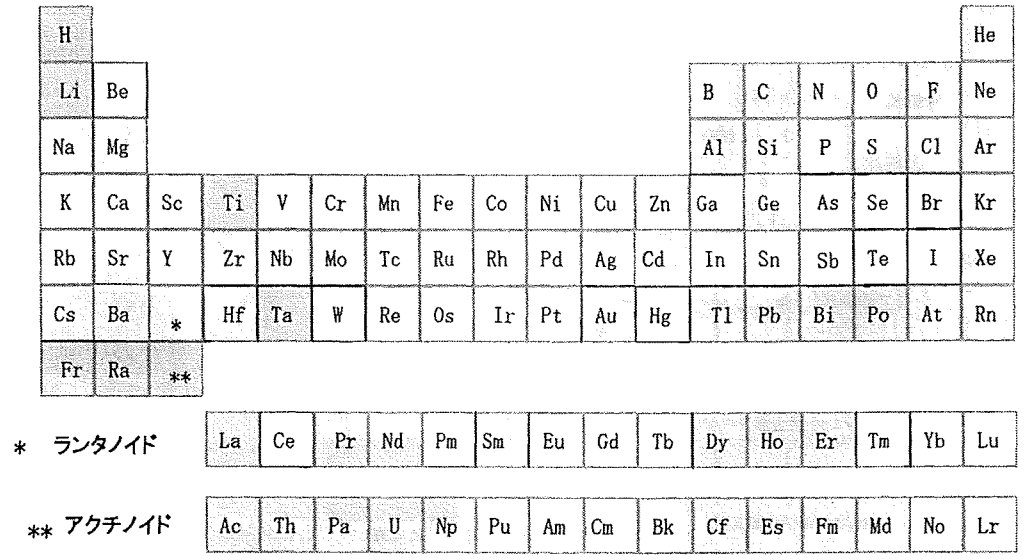

図 3 マルチトレーサ中に含まれる γ 線放出核種　シャトーのついている元素はマルチトレーサ中に含まれている。照射ターゲットは，Ti，Fe，Cu，Ge，Ag 及び Au などを利用する

験を行ったところ，γ線スペクトロメトリーによって^{24}Naから^{61}Cuまでの18元素50核種のRIが利用可能であった。ガスジェット結合型多重標的照射室を貫いたビームは，長寿命RIの製造を目的とした照射室に入る。ここでは，厚さ200 μm程度のチタン，銀や金などの標的が数枚照射される。標的は，水とヘリウムガスによって効率的に冷却され，最大700 pμAの^{14}Nビーム強度まで照射実績がある。照射後，標的物質を化学的手法によって除去すれば，マルチトレーサ溶液が得られる。

4 マルチトレーサ法の特長

マルチトレーサ法には様々な特長がある。まず，第1は高能率化である。すなわち，1回の実験で十数種から数十種の元素について情報が得られる。その波及効果として，これまでトレーサの利用が考えられなかった新しい対象への適用が考えられる。例えば，ある系で一定の挙動を示す元素を探したいとする。従来のトレーサ法では1つ1つの元素についてRIトレーサを入手し，次々と実験していかなければならない。これに対してマルチトレーサを利用すれば，1回の実験で目的を果たすことができる。第2には，これらの情報が完全に同一の条件下で得られることである。多数の元素の挙動を比較する場合，これまでのシングルトレーサ法では，個々の元素について別々に実験して得られたデータを基に議論されてきた。多くの場合，別々のグループにより報告されたデータが集められ，考察の基礎とされてきた。しかし，これは多くの場合かなり問題で，試料差，個体差の大きい地球環境試料や生体試料については，マルチトレーサ法によって，同時に完全に同一の条件下で多数の元素についてデータが得られることは，それらの相互比較において極めて重要である。第3には，マルチトレーサ法では，RIが無担体で得られることである。RIの放出する放射線は高い感度で検出できることから，トレーサとして使用する際には，pgのオーダーで十分である。しかし，原子炉から得られるRIは，ある量の安定同位体（担体）と共存するため，使用する元素の量自体はこれよりはるかに多くなる。AsやHgのように毒性の強い元素を正常な個体に投与して追跡しようとするとき，これは大きな問題になる。この点，マルチトレーサ法では，RIだけを投与できるため，投与量が微量ですみ，毒性をほとんど無視することができる。逆に，担体が含まれるほうが好ましい実験では，これを加えることは容易である。第4には，マルチトレーサは意外な発見の可能性，いわゆるセレンディピティーを持っていることである。多くの元素について，“情報が得られてしまう”ため，必ずしも意図していなかった元素について予想もしなかった新しい事実が見つかる可能性がある。これは，個々に入手したRIを自分で混ぜたのでは起こり得ないことである。さらに，マルチトレーサは現在でも50種類を超える元素に適用可能で，今後その数はさらに増加していくはずであるが，既に，シングルトレーサとしても貴重な^{28}Mgや^{47}Caなどを含んでいる。^{28}Mgは実用性のあるMgのトレーサとしては唯一のものであるが，一般には供給されていない。Caのトレーサとしては^{45}Caが広く使われているが，このRIはほとんどγ線を放出せず，β線測定をしなければならない。これに対して^{47}Caはγ線放出体であるので，多くの実験で極めて有利である。

5 最近の応用研究

マルチトレーサの応用研究は，多くの分野にわたっており，今日も多くの研究成果が出されている。2005年までの成果は，既に総説で紹介しているので[2]，これ以降の応用研究について簡単に紹介したい。

昭和薬科大学の松本謙一郎（現 放射線医学総合研究所）らは，高純度Ge半導体検出器に鉛のコリメータを装着し，ラットに銀由来のマ

ルチトレーサを投与し，その個体を生きたままの代謝過程追跡実験を行い，複数核種の検出効率を求めた。一般にマルチトレーサのユーザーは，動物に投与後，経時的に解剖を行い，それぞれの臓器分布を測定することが多いが，GREIの開発にも有益な基礎データを提供した論文として興味深い[7]。金沢大学の金山洋介（現 理化学研究所神戸・分子イメージング）らは，マウスにおけるRbとTlの嗅覚輸送系を利用した脳内RI投与経路に関する研究を報告している[8]。彼らは，鼻腔粘膜上にマルチトレーサを投与し，嗅神経系を介した軸索輸送過程を脳の詳細な分布測定で再構成することに成功している。一方，昭和薬科大学の近藤昌夫（現大阪大学薬学部）らのグループは，妊娠時における胎児と母体の亜鉛輸送に関する一連の実験系で，ヒトトロブラストBeWo細胞におけるフォルスコリンにより亜鉛輸送の誘導に関する研究を行い亜鉛トランスポーター1,2及び4のメッセンジャーRNAレベルがフォルスコリンの投与で上昇することを示し，胎盤の分子生物学的研究のアプローチにおける亜鉛輸送の研究に有益な実験系であることを証明している[9]。静岡大学の矢永誠人らのグループは，亜鉛欠乏マウスにおける肝臓の蛋白質分画を詳細に行い，マルチトレーサにより投与された元素の分布状態を明らかにしている[10]。また，栄養学の研究では，理研の五十嵐香織らが，鉄欠乏貧血に対する鉄強化剤としてNaFeEDTAを使用した場合のほかの必須元素の取り込みに対する影響を検討し，NaFeEDTAの有用性を証明した[11]。さらに，前に述べたように理研の本村信治らは，GREI装置による世界初の複数分子同時イメージングの成功を報告している[5,6]。環境科学の分野の研究では，広島大学の高橋嘉夫らのグループが，海水と海底沈降物におけるReとOsの還元的条件における蓄積について，マルチトレーサ法で検討した報告がある[12]。すなわち，ReとOsの海水中での存在度と濃縮のメカニズムはいまだに理解されていないが，実験室において人工海水－東京湾堆積物間におけるReとOsの吸着挙動を^{183}Reと^{185}Osを含んだマルチトレーサを用いて調べた他にも様々な応用研究が進められ，マルチトレーサ法にXAFS法を組み合わせることによってReとOsの化学種の同定を行い，海水-堆積物系における還元的集積メカニズムを明らかにした。また，同じく広島大学の高橋嘉夫らのグループは，土壌-水間における様々な元素のダイナミクスを解明するため，マルチトレーサ法とICP-MS法を組み合わせたユニークな実験手法を確立した[13]。他にも多くの応用研究の報告もあるが今後，マルチトレーサ研究は分子イメージング研究を含めた，広い応用研究が進められていくことであろう。

マルチトレーサならびにGREIの研究には，文部科学省科学研究費，厚生労働省科学研究費，NEDO研究費などの研究費により遂行された。

参考文献

- N. Lowe, and M. Jackson, Eds., Advances in Isotope Methods for the Analysis of Trace Elements in Man, CRC Press, Washington, D. C., (2001)
- F. Ambe, S. Ambe, and S. Enomoto, Tracer Technique, 443-474, A. Vertes, S. Nagy, Z. Klencsar, Eds., Chemical Applications of Nuclear Reaction and Radiation, Kluwer Academic Publishers, London, (2003)
- A. Vertes, S. Nagy, Z. Klencsar, Eds., Radiochemistry and Radiopharmaceutical Chemistry in Life Sciences, Kluwer Academic Publishers, London, (2003)
- 榎本秀一，多元素同時分析法としてのマルチトレーサ法とその応用研究およびRIビームファクトリー計画における新展開，*RADIOISOTOPES*, **52**, 631-647(2003)
- D. Nayak, *Appl. Radiat. Isotopes*, **54**, 195(2001)

引用文献

1) S. Ambe, S. Y. Chen, Y. Ohkubo, Y. Kobayashi, M. Iwamoto, M. Yanokura, and F. Ambe, Preparation of radioactive multitracer solution from gold foil irradiated by 135 MeV/nucleon 14N ions, *Chem. Lett.*, 149-152(1991)

2) 榎本秀一，多元素同時分析法としてのマルチ

トレーサー法とその応用研究およびRIビームファクトリー計画における新展開, *RADIOISOTOPES*, **52**, 631–647(2003). および S. Enomoto, Development of Multitracer Technology and Application Studies on Biotrace Element Research. *Biomed. Res. Trace Elem.* **16**, 233–240(2005)

3) H. Haba, D. Kaji, Y. Kanayama, K. Igarashi, and S. Enomoto, Development of a gas-jet-coupled multitarget system for multitracer production, *Radiochim. Acta*, **93**, 1–4(2005)

4) S. Shibata, K. Takamiya, T. Ichihara, and T. Sasaki, Separation of radionuclides in a multitracer prepared by thermal neutron fission of ^{235}U, *Appl. Radiation Isotopes*, **60**, 625–628(2004)

5) S. Motomura, S. Enomoto, H. Haba, K. Igarashi, Y. Gono, Y. Yano, Gamma-ray Compton imaging of multitracer in biological samples using strip germanium telescope, *IEEE Transaction on Nuclear Science*, **54**(3), 710717(2007)

6) S. Motomura, Y. Kanayama, H. Haba, Y. Watanabe, and S. Enomoto, Multiple Nuclide Imaging in Live Mouse Using Semiconductor Compton Camera for Multiple Molecular Imaging, *J. Anal. Atom. Spectrom.*, in press

7) K. Matsumoto, R. Hirunuma, S. Enomoto, K. Endo, *In vivo* multitracer analysis technique: Screening of radioactive probes for noninvasive measurement of physiological functions in experimental animals. *Biol. Pharm. Bull.*, **28**, 2029–2034(2005)

8) Y. Kanayama, S. Enomoto, T. Irie, R. Amano, Axonal transport of rubidium and thallium in the olfactory nerve of mice, *Nucl. Med. Biol.*, **32**, 505–512(2005)

9) N. Asano, M. Kondoh, C. Ebihara, M. Fujii, T. Nakanishi, N. Utoguchi, S. Enomoto, K. Tanaka, Y. Watanabe, Induction of zinc transporters by forskolin in human trophoblast BeWo cells, *Reproductive Toxicology*, **21**, 285–291(2006)

10) R. Minayoshi, T. Ohyama, N. Kinugawa, J. Kamishima, T. Ogi, K. Ishikawa, M. Noguchi, H. Suganuma, K. Takahashi, S. Enomoto and M. Yanaga, Change of concentrations of trace elements and protein contents in the liver of zinc deficient mice, *Journal of Radioanalytical and Nuclear Chemistry*, **272**(2), 429–431(2007)

11) K. Igarashi, Y. Nakanishi, R. Hirunuma, S. Enomoto, S. Kimura, Multitracer study on the uptake of various trace elements in anemic rats: influence of NaFeEDTA and ferrous sulfate, *Nutrition Research*, **26**, 173–179(2006)

12) Y. Yamashita, Y. Takahashi, H. Haba, S. Enomoto, H. Shimizu, Comparison of reductive accumulation of Re and Os in seawater - sediment systems, *Geochimica et Cosmochimica Acta*, **71**(14), 3458–3475(2007)

13) S. Mitsunobu, Y. Takahashi, R. Hirunuma, H. Haba, S. Enomoto, *Chem. Lett.* **34**, 980–981(2005)

Imaging【イメージング】

複数分子の同時イメージングを実現した世界初の診断装置を開発

近年，病気の診断・治療の場において，分子イメージング技術が大きな力を発揮している。しかし，現在汎用されているPETやMRIなどの診断装置では，さまざまな分子の動きを同時に画像化することはむずかしかった。複数の要因が複雑かつ複合的に関与して発症するがんやさまざまな生活習慣病などの診断をより高度におこなうために，複数分子の同時イメージング技術が切望されていた。このほどマウスでの成功が発表され，新たな創薬や診断法の革新に向けて，実用装置としての開発が加速している。

分子イメージングにおける複数分子同時イメージングのメリット

わが国や欧米諸国では，分子イメージング研究を国家的に推進しており，ポジトロン断層診断装置（PET）などの分子イメージング機器を用いて，生体のさまざまな反応や疾患の分子レベルの情報が，定量性をもった画像として得られるようになってきた。たとえば，がんをはじめとする病態などの早期診断や研究にPETが汎用され，優れた核医学診断装置として活躍している。しかし，PETの検出器は放射性薬剤が陽電子崩壊の際に発する511keVのγ（ガンマ）線だけを利用するため，核種ごとに異なるγ線を識別して，複数の放射性薬剤を同時にイメージングすることができない。

がんやさまざまな生活習慣病などの疾病には，複数の要因が複雑かつ複合的に関与していることが明らかになっている。それぞれの要因に対して特異性をもつ複数の分子プローブを同時に用いることができると，疾病の複雑なメカニズムやほかの生体反応との相互作用がイメージングでき，より高度で正確な診断が可能になる。

われわれは，放射性医薬品を利用した診断，治療の分野の分子イメージング装置として，高純度ゲルマニウム半導体検出器を用いたコンプトンカメラ[*1]方式の「複数分子同時イメージング装置（Gamma ray emission imaging：GREI）」を開発してきた[(1)]。

この装置は，検出器としてゲルマニウム半導体を使っているため，エネルギー分解能[*2]がとくに優れている。このため，それぞれ異なる放射性同位元素で標識した複数の放射性薬剤（分子プローブ）を同時に用いれば，GREIは放出されるγ線のエネルギーを精密に計測できるため，そのエネルギーを指標として各々の分子を識別することができる。

図1　複数分子同時イメージング装置「GREI」の撮像原理（a）とGREI装置（b）

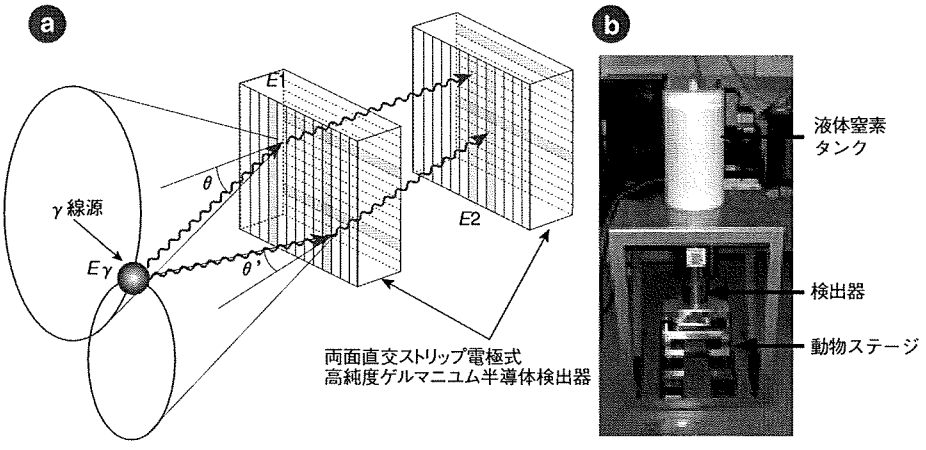

GREIのセンサーは両面直交ストリップ電極式の高純度ゲルマニウム半導体検出器であり，入射γ線の相互作用位置とエネルギーを高精度に測定することが可能になっている。コンプトン散乱事象[*1]を一つ検出すると，コンプトン散乱の方程式を解いてその散乱角度が求められ，図中の一つの円錐上のどこかにγ線源が存在することがわかる。このような円錐の情報を多数集めるとγ線源の場所が特定でき，薬剤の分布画像を推定することが可能となる。

図2　GREIで同時に撮像した3種類の放射性薬剤の複合画像

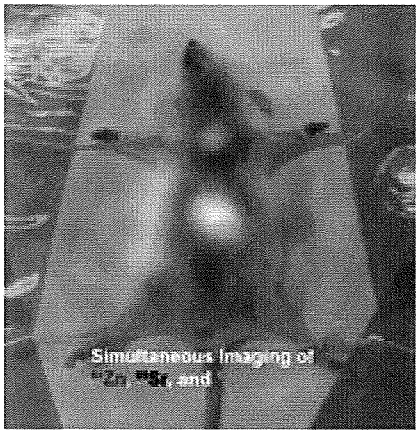

放射性薬剤ごとに色分けして一つの画像にすることで，複合的な情報を視覚的に表現することが可能である。分布が重なった部分は，色の混合により異なる色で表現される。

＊1　コンプトンカメラ
コンプトン散乱の運動学を利用して，γ線源の放射能密度分布を画像化する装置の総称。一般的に，散乱体と吸収体の複数の半導体検出器などを並べることにより実現される。原理的に，1方向からの撮像により3次元の密度分布を画像化することが可能である。コンプトン散乱は，1923年にアーサー・コンプトンによって確かめられた，光(電磁波)による電子の散乱現象。散乱前の光のもつエネルギーが既知であれば，散乱の角度により，散乱後の光および電子のもつエネルギーは，運動学的に一意に決定できる。光の粒子性を示す現象の一つである。

＊2　エネルギー分解能
エネルギー値の異なる二つの放射線について，どのくらいの差まで区別して測定できるかという能力をいう。エネルギー分解能が高いと，分子プローブの識別能が向上するだけでなく，γ線の散乱角の推定精度も向上するため，コンプトンカメラにとってはとくに重要な要因である。ゲルマニウムはきわめて高純度の半導体単結晶を形成させることが可能で，大体積の放射線検出器として動作させることができ，ほかの放射線検出器と比較してエネルギー分解能がきわだって優れている。

＊3　ICR系統マウス
毒性・薬理・薬効・免疫・その他の試験など幅広い分野で汎用的に使用されるマウス。アメリカのInstitute of Cancer Researchの頭文字をとって命名された。

GREIに設置した二つの検出器（**図1**）の寸法は，縦横が39mm×39mm，厚さは前段が10mm，後段が20mmで，検出器間の距離は60mmとなっている。この検出器の電極は，表と裏で互いに直交する方向で3mm周期のストリップ状に分割しているため，さまざまな方向から飛来するγ線の相互作用位置をXY方向について検出することができる。さらに検出器の厚みの方向，Z方向についても，約1mmの検出精度を達成している。また，コンプトンカメラはγ線の入射方向を制限しないため，1方向からの固定撮像でも3次元分布の情報が得られるという特徴がある。

複数分子同時イメージングの実現

われわれは，このGREIを用いて，複数分子同時イメージングを実証するため，健常マウスに分子プローブとして複数の放射性薬剤を投与した代謝過程のイメージング実験をおこなった。

すなわち，ICR系統マウス[*3]（8週齢・雄）に，3種類の放射性薬剤を連続投与し，麻酔をした状態でGREIを作動させ12時間の連続撮像をおこなった。投与した薬剤は，ヨウ化メチルノルコレステノール（^{131}I）注射液（アドステロール®-I131注射液），塩化ストロンチウム（$^{85}SrCl_2$），塩化亜鉛（$^{65}ZnCl_2$）で，それぞれ副腎，骨，肝臓に集積性をもつ。

GREIで測定したγ線エネルギースペクトルから，それぞれの放射性薬剤が明確に識別できていることがわかり，この撮像実験で得られたデータから，2次元および3次元画像化し，それぞれの放射性薬剤ごとに解析をおこなった。マウスの光学カメラ画像と放射性薬剤の分布を重ね合わせ，薬剤ごとに色分けし，複合画像を**図2**に示す。

図3　同時投与した3種類の放射性薬剤の時系列連続画像

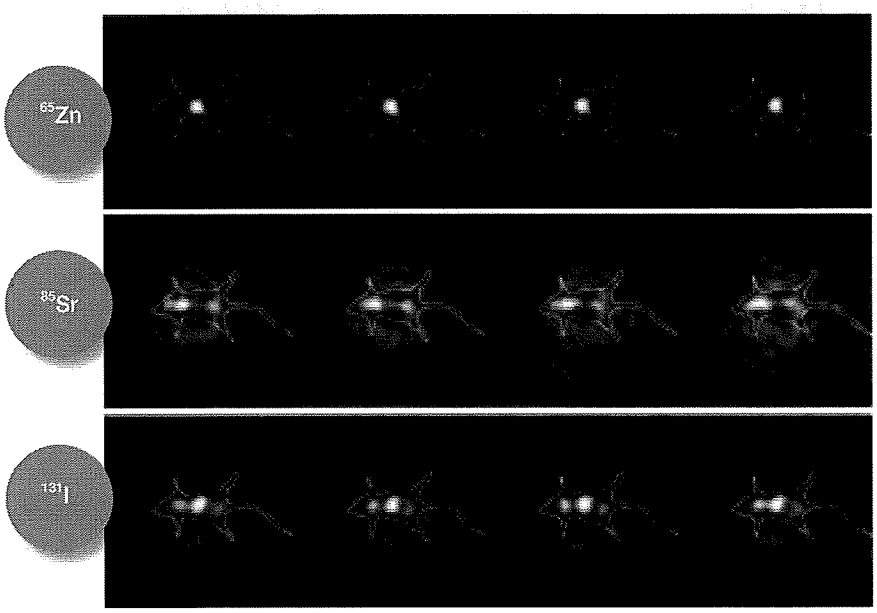

GREIの撮像データには時刻の情報が組み込まれており，撮像後に時間範囲を自由に設定して連続画像を生成することができる。図は，3時間ごとにデータを区分して画像生成した例。

また，このGREI撮像実験では，リアルタイムイメージングのための実証実験にも成功した(**図3**)。

このようなイメージング技術は，われわれが世界に先駆けて1999年から開発を進めてきたもので，今回世界で初めて，複数放射性薬剤同時リアルタイムイメージングに成功した。

今後の展開

臨床医学の現場で，複数分子同時イメージング法が活用されるには，分子プローブに用いる放射性薬剤の開発も重要である。2008年10月，われわれが中心となって，京都大学，大阪大学，宇宙航空研究開発機構の研究グループと放射性薬剤開発を加速し，コンプトンカメラによる新診断機器開発を推進するコンソーシアムを発足した。

このようなコンプトンカメラ方式による複数分子同時イメージング法の実用化に対する取り組みは，わが国が世界をリードしており，近い将来，実用的な診断機器が創出されることは疑いがない。われわれは現在，要素技術をさらに高度化し，解像度が1mm以下となる，より実用的な撮像をめざして開発を進めている。このような装置開発と新薬の開発研究を活性化し，複数分子同時イメージング法による創薬や診断法の革新に貢献していきたい。

榎本秀一　えのもと・しゅういち

岡山大学　大学院医歯薬総合研究科　創薬生命科学専攻　教授。理化学研究所　神戸研究所　分子イメージング科学研究センター　メタロミクスイメージング研究ユニット　研究ユニットリーダー。
1991年北海道大学大学院薬学研究科博士後期課程修了，薬学博士。日本学術振興会PD，理化学研究所基礎科学特別研究員，理化学研究所仁科加速器研究センター副チームリーダーなどを経て，2008年10月から現職。メタロミクス研究と分子イメージング研究を推進中。

参考文献

[1] Motomura S et al："Gamma-ray Compton imaging of multitracer in biological samples using strip germanium telescope" IEEE Trans Nucl Sci 54 (2007) 710-717
[2] Motomura S et al："Multiple molecular simultaneous imaging in a live mouse using semiconductor Compton camera" J Anal At Spectrom 23 (2008) 1089-1092

Journal of Neuroscience Research 86:929–936 (2008)

Up-Regulated Neuronal COX-2 Expression After Cortical Spreading Depression Is Involved in Non-REM Sleep Induction in Rats

Yilong Cui,[1,2,3] Yosky Kataoka,[1,3,4]* Takashi Inui,[5] Takatoshi Mochizuki,[5] Hirotaka Onoe,[1,3] Kiyoshi Matsumura,[3] Yoshihiro Urade,[5] Hisao Yamada,[2] and Yasuyoshi Watanabe[1,3,4]

[1]Molecular Imaging Research Program, Institute of Physical and Chemical Research (RIKEN), Kobe, Hyogo, Japan
[2]Department of Anatomy and Cell Science, Kansai Medical University, Moriguchi, Osaka, Japan
[3]Department of Neuroscience, Osaka Bioscience Institute, Suita, Osaka, Japan
[4]Department of Physiology, Osaka City University Graduate School of Medicine, Abeno-ku, Osaka, Japan
[5]Department of Molecular Behavioral Biology, Osaka Bioscience Institute, Suita, Osaka, Japan

Cortical spreading depression is an excitatory wave of depolarization spreading throughout cerebral cortex at a rate of 2–5 mm/min and has been implicated in various neurological disorders, such as epilepsy, migraine aura, and trauma. Although sleepiness or sleep is often induced by these neurological disorders, the cellular and molecular mechanism has remained unclear. To investigate whether and how the sleep-wake behavior is altered by such aberrant brain activity, we induced cortical spreading depression in freely moving rats, monitoring REM and non-REM (NREM) sleep and sleep-associated changes in cyclooxygenase (COX)-2 and prostaglandins (PGs). In such a model for aberrant neuronal excitation in the cerebral cortex, the amount of NREM sleep, but not of REM sleep, increased subsequently for several hours, with an up-regulated expression of COX-2 in cortical neurons and considerable production of PGs. A specific inhibitor of COX-2 completely arrested the increase in NREM sleep. These results indicate that up-regulated neuronal COX-2 would be involved in aberrant brain excitation-induced NREM sleep via production of PGs.

Key words: aberrant excitation; prostaglandin; spreading depression; sleep; cyclooxygenase-2

Cortical spreading depression (SD) was described first by Leao (1944), and characterized by a transient negative shift of direct current (DC) potential (Nedergaard and Hansen, 1988) and temporal elevation of cerebral blood flow (CBF; Fabricius et al., 1995; Shimizu et al., 2000). It is due to a self-propagating front of depolarization that begins in the neuronal and/or glial cells of local areas of the brain and subsequently spreads in all directions at a rate of approximately 2–5 mm/min (Leao, 1944; Shinohara et al., 1979; Hansen and Zeuthen, 1981; Lauritzen et al., 1982). SD has been implicated in the pathophysiological states of various neurological disorders, such as epilepsy, migraine aura, and trauma (Gorji, 2001), which are accompanied by an aberrant neuronal excitation in the brain. Although it is well known empirically that sleepiness or sleep is often induced by these neurological disorders (Sand, 1991; Donnet and Bartolomei, 1997; Foldvary, 2002), the cellular and molecular mechanism of the sleep induction has remained unclear.

Cyclooxygenase (COX)-2 is now known to be constitutively expressed in the central nervous system in restricted neuronal populations, including cerebral cortical and hippocampal neurons. Neuronal COX-2 expression is regulated by neural activity, such as synaptic activity or membrane depolarization accompanied by Ca^{2+} loading in cells (Koistinaho and Chan, 2000; Yermakova and O'Banion, 2000), and its expression is dramatically increased in a variety of neurological disorders, such as epilepsy, migraine aura, and trauma (Yamagata et al., 1993; Nogawa et al., 1997; Strauss et al., 2000). COX-2 is a rate-limiting enzyme of the arachidonic acid cascade and triggers production of prostaglandins (PG) and other related substances. PGs play important and diverse roles

Contract grant sponsor: Ministry of Education, Culture, Sports, Science and Technology of the Japanese Government (to Y.K.); Contract grant sponsor: Japan Society for the Promotion of Science; Contract grant number: 16700291 (to Y.C.).

*Correspondence to: Yosky Kataoka, Department of Physiology, Osaka City University Graduate School of Medicine, 1-4-3 Asahimachi, Abeno-ku, Osaka 545-8585, Japan. E-mail: kataokay@med.osaka-cu.ac.jp

Received 19 June 2007; Revised 24 July 2007; Accepted 26 July 2007

Published online 10 October 2007 in Wiley InterScience (www.interscience.wiley.com). DOI: 10.1002/jnr.21531

in the central nervous system. A variety of central actions have been demonstrated, such as regulation of sleep-wake cycle (Hayaishi, 1988; Hayaishi and Urade, 2002), body temperature (Ueno et al., 1982), and luteinizing hormone-releasing hormone (LHRH) secretion (Ojeda et al., 1982) and potentiation of the action of excitatory amino acids on Purkinje cell dendrites (Kimura et al., 1985). These observations raise the possibility that up-regulated neuronal COX-2 after aberrant neuronal excitation in these neurological disorders is involved in sleep induction via triggering production of PGs; however, no literature has clarified this.

To investigate whether and how the sleep-wake behavior is altered by aberrant brain activity, we induced cortical SD in freely moving rats and investigated the functional role of neuronal COX-2 in sleep induction. SD can be remotely induced in the animals under the freely moving condition, by photodynamic oxidation of a local region of the cerebral cortex using a glass fiber (Kataoka et al., 2000; Cui et al., 2003). Here we provide a new line of evidence that neuronal COX-2 is involved in signal regulation of non-REM (NREM) sleep induction after aberrant neuronal excitation in the cerebral cortex.

MATERIALS AND METHODS

All experimental protocols were approved by the Ethics Committee on Animal Care and Use of Kansai Medical University and were performed in accordance with the *Principles of laboratory animal care* (NIH publication No.85-23, revised 1985).

Animal Preparation for Generation of Spreading Depression in Freely Moving Rats

Cortical SD was generated in freely moving male Sprague-Dawley rats (weighing about 300 g; SLC, Hamamatsu, Japan) using the photodynamic tissue oxidation (PDTO) technique (Kataoka et al., 2000; Cui et al., 2003). The animals were housed before experimentation in a soundproof chamber (ambient temperature 25°C, relative humidity 60%). The chamber was maintained on a 12:12-hr light:dark cycle (lights on at 8 AM), and standard laboratory rat chow and water were supplied ad libitum. The animals were anesthetized with 4.0% halothane, and anesthesia was maintained with 1.0% halothane in air. The head of each animal was fixed in a stereotaxic apparatus (type 1430; David Kopf, Tujunga, CA). A small burr hole for injection of rose Bengal was drilled in the skull at the frontal cortex (2.0–3.0 mm anterior and 2.0–3.0 mm lateral to the bregma). Then, rose Bengal (3 mM, 1.6 μl) was injected through a glass micropipette (internal diameter of the tip 50 μm) into the frontal cortex (0.5–2.0 mm ventral to the cortical surface) taking 40 min in a dark room. A short plastic cannula for guiding the tip of a glass fiber on the rose Bengal-injected area was fixed on the burr hole by instant adhesive. A plug was kept in the cannula to prevent photoactivation of rose Bengal by room light before the experiments.

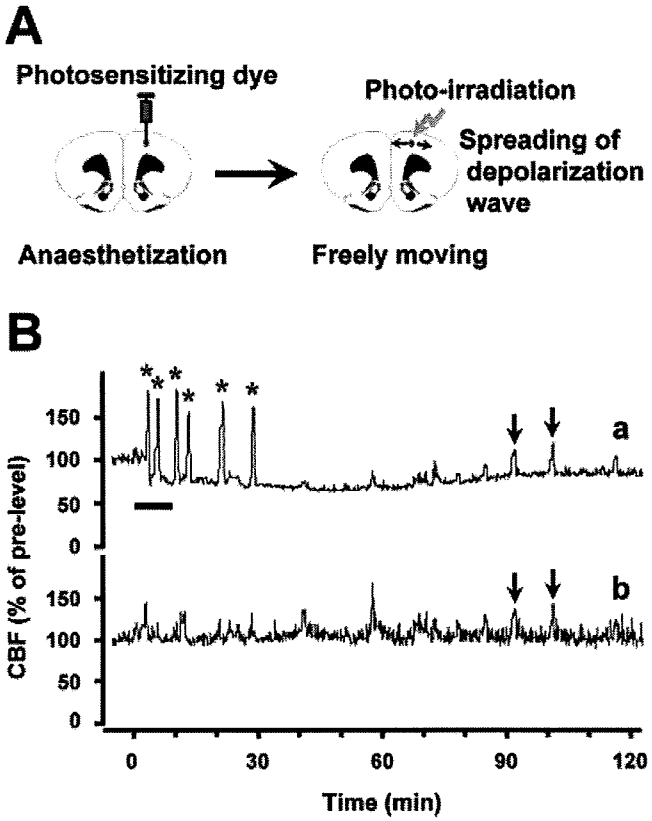

Fig. 1. Cortical spreading depression (SD) in freely moving rats. **A:** The photodynamic tissue oxidation (PDTO) procedure for inducing SD in the cortical hemisphere of a freely moving rat. **B:** Cerebral blood flow (CBF) changes in a freely moving animal. Two laser Doppler flowmeter (LDF) probes were placed [one on the parietal cortex of the PDTO-treated brain hemisphere (a) and one on the opposite side (b)]. While the animal was freely moving, the rose Bengal-injected site in the frontal cortex was photoirradiated (540–580 nm and 380 mW/cm^2) via a glass fiber. Bar in the upper panel indicates photoirradiation lasting 10 min. Asterisks indicate SD-associated hyperperfusion events. Note that some irregular fluctuations of the CBF, indicated by an arrow, were concomitantly observed in both hemispheres.

Cerebral Blood Flow Recording

Five of the rose Bengal-injected rats were used for recording cerebral blood flow (CBF). The CBF was detected with laser Doppler flowmetry (LDF; type FLO-N1; Omegawave, Tokyo, Japan). Immediately after the rose Bengal injection, one LDF probe (0.2 mm diameter) was inserted into each of two small burr holes (previously drilled in the skull, 7 mm posterior to the dye-injected area and on the hemispherically opposite side). The plastic cannula and LDF probes were rigidly fixed to the skull with dental acrylic cement, and two screws anchored them to the skull. The rats were returned to their cages for 3–4 hr and allowed free movement. The plug in the plastic cannula was replaced with a glass fiber (1 mm diameter), and the rose Bengal-injected area was photoirradiated (metal halide lamp, 540–580 nm, and 380 mW/cm^2) via the glass fiber (see Fig. 1A). The laser Doppler flowmeter

does not measure actual perfusion units, so percentage of change in CBF was determined (the data were normalized to 5 min of pre-PDTO values).

Sleep Monitoring

The vigilance stages were monitored in 15 rose Bengal-injected and 6 vehicle-injected rats using EEG and electromyography (EMG). Because SD reduces cortical EEG amplitude (Leao, 1944) in the treated hemisphere by causing a transient membrane depolarization in the neurons, we recorded EEG signals from the opposite hemisphere. Immediately after the rose Bengal injection, three Teflon-coated stainless-steel wire electrodes bared at the tip were chronically implanted into the parietal cortex of the hemisphere opposite to the dye-injected cortex for EEG recordings. A stainless-steel screw attached to the frontal region of the skull served as the ground electrode. Two stainless-steel wire electrodes were inserted into the neck muscles for EMG recordings. The plastic cannula and electrodes were rigidly fixed to the skull with dental acrylic cement, and three screws anchored them to the skull.

After housing each animal in the experimental chamber for 3 days, the plug in the plastic cannula was replaced with a glass fiber (1 mm diameter), and the 24-hr polygraphic recordings of EEG and EMG were started at 2 PM. The rose Bengal-injected area was photoirradiated at 8 PM according to the same protocol used for generation of SD described above. At the end of the recording time, animals were perfused with 4% formaldehyde buffered with 0.1 M phosphate-buffered saline (PBS; pH 7.4) under deep anesthesia with diethyl ether. Then, a histological study was performed to check the position of EEG electrodes in the cerebral cortex.

The EEG/EMG signals were amplified, filtered (EEG 0.5–20 Hz, EMG 20–200 Hz), and recorded with a sampling rate of 128 Hz. The data were analyzed using an animal sleep analysis software package (SleepSign; Kissei Comtec, Matsumoto, Japan); the behavioral states of the animals were automatically classified into one of three stages (i.e., wakefulness, NREM, or REM sleep) every 4 sec, according to the standard criteria (Tobler et al., 1997; Gerashchenko et al., 2000; Huang et al., 2001). The automatically defined stages were verified by researchers.

PG Enzyme Immunoassay

Fifteen male Sprague Dawley rats were used for PG enzyme immunoassay. At 2 hr after onset of SD (induced by photooxidation for 30 min), rats were killed by an overdose of diethyl ether anesthesia. The heads were immediately frozen in liquid nitrogen. The whole brain was rapidly removed, weighed, and then homogenized in ethanol (pH 2.0) containing 0.02% HCl. The material was centrifuged at 500*g* for 20 min. ^{3}H-labeled PGD_2, PGE_2, and $PGF_{2\alpha}$ (60 Bq for each assay; New England Nuclear, Boston, MA) were added as tracers for estimating recovery to the supernatant. The PGs were extracted with ethyl acetate, which was evaporated under nitrogen, and then the samples were separated by HPLC as described previously (Pandey et al., 1995). The quantification of PGs was performed with enzyme immunoassay (EIA) using their EIA kits (Cayman Chemical, Ann Arbor, MI).

Immunohistochemistry

Localizations of COX-2 and lipocalin-type PGD synthase (L-PGDS) in the brain were immunohistochemically examined in five other rats. Two hours after onset of SD, each rat (under deep anaesthesia with diethyl ether) was perfused with 4% formaldehyde buffered with 0.1 M phosphate-buffered saline (PBS; pH 7.4). The brain was removed and further fixed in the same fixative for 24 hr at 4°C. We prepared coronal brain sections (30 μm thickness) using a cryostat and performed immunohistochemical studies. To immunostain COX-2, rabbit polyclonal antibody recognizing rat COX-2 (1:2,000; Cayman Chemical) was used. The bound antibodies were visualized by the avidin-biotin complex method (Vectastain ABC kit; Vector, Burlingame, CA). Double immunofluorescence staining of COX-2 and L-PGDS was carried out by a series of immunoreactions, first with rabbit polyclonal antibody recognizing rat L-PGDS (1:200), which was visualized by Cy2-conjugated secondary antibody (Jackson Immunoresearch, West Grove, PA) and then with rabbit polyclonal antibody recognizing rat COX-2, which was visualized by Cy5-conjugated secondary antibody (Jackson Immunoresearch). A confocal laser microscope (Zeiss LSM 510; Carl Zeiss, Oberkochen, Germany) was used for observation.

RESULTS

Spreading Depression in Freely Moving Rats

CBF was monitored after surgery at a site 7 mm posterior to the dye-injected area and at the corresponding site in the opposite hemisphere. After recovery from anesthesia, some irregular fluctuations of CBF were concomitantly recorded from both hemispheres (Fig. 1B). Such transient CBF changes are thought to reflect changes in local brain activities in freely moving animals. After placing each animal in the experimental chamber for 3–4 hr, the rose Bengal-injected area was photooxidized for 10 min. Beginning several minutes after the onset of photooxidation, changes in CBF [with amplitudes that were 71.7 ± 4.1% (mean ± SEM, n = 30 deflections in 5 animals) of that before photooxidation] were observed for approximately 1 hr in the photooxidized hemisphere but not in the opposite hemisphere, as is characteristic of SD (Cui et al., 2003). Such transient CBF changes are well known to be synchronously accompanied by the transient negative shifts of DC potential, as described in our previous report (Cui et al., 2003) and in other studies (Back et al., 1994; Gold et al., 1998). The small spontaneous fluctuations of CBF disappeared during the PDTO-induced SD in the photooxidized hemisphere. During the photooxidation and SD, the animals showed hypoactivity but not show hemiparalysis nor convulsion.

Increase in NREM Sleep Induced by Cortical SD

Sleep-wake behavioral states in freely moving rats, i.e., experimental (photoirradiated following rose Bengal

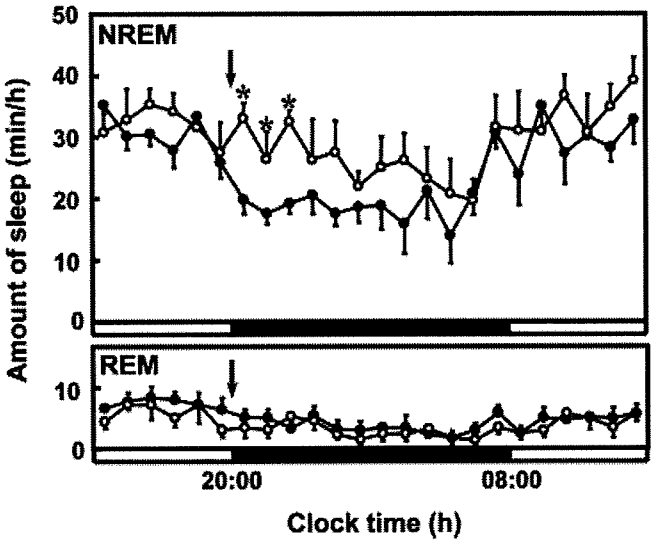

Fig. 2. Cortical spreading depression (SD)-induced NREM and REM sleep. Hourly changes of amounts of NREM sleep (NREM) and REM sleep (REM) were plotted for 24 hr (starting at 2 PM) in SD-induced (open circles, n = 5) and sham-operated (vehicle-injected) animals (solid circles, n = 6). Arrows indicate the 10-min photoirradiation period. $*P < 0.05$, two-way ANOVA, Scheffe's multiple-comparison procedure.

injection; n = 5 animals) and sham-operated (photoirradiated following vehicle injection; n = 6 animals), were evaluated on the basis of EEG and EMG criteria. The sham-operated animals exhibited a normal circadian reduction in the amount of NREM sleep during the dark period; the amount of NREM sleep decreased to approximately 18 min/hr (8 PM – 8 AM, dark) from 30 min/hr (8 AM – 8 PM, light). However, the amount of NREM sleep in the experimental relative to that in the sham-operated rats significantly increased for 3 hr following SD induction ($P < 0.05$, two-way ANOVA, Scheffe's multiple-comparison procedure; Fig. 2A). No significant differences in amount of REM sleep were noted between the experimental and sham-operated animals following SD induction ($P < 0.05$, two-way ANOVA, Scheffe's multiple-comparison procedure).

Neuronal COX-2 Expression and Production of PGs by Cortical SD

The COX-2 immunoreactivity was dramatically increased in neurons of layers II and III, with moderate expression in all the other cortical layers in the SD-induced cortical hemisphere (Fig. 3). Small numbers of COX-2-immunopositive neurons were scattered throughout the contralateral hemisphere and on both sides of the cerebral cortex of the untreated animals, indicating moderate constitutive expression of the enzyme in cortical neurons. Enzyme immunoassay on whole brain showed that the amounts of PGD_2, PGE_2, and $PGF_{2\alpha}$ in nontreated animals (n = 5 animals) were

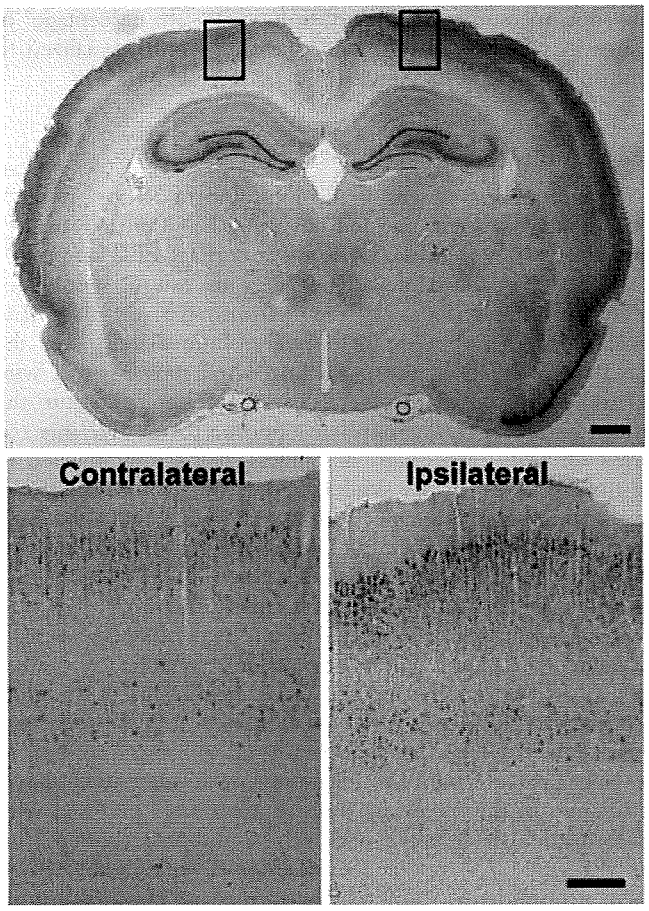

Fig. 3. Cortical spreading depression (SD) induced COX-2 expression in cortical neurons. Upper panel: Coronal view of the midcortex (a coronal section at 5 mm posterior to photooxidized area). Marked COX-2 immunoreactivity in cortical neurons of the hemisphere (the right side) 2 hr after onset of SD. Lower panel: Magnified views of areas indicated by the left (contralateral) and the right (ipsilateral) rectangles in upper panel. Scale bars = 1 mm in upper panel; 200 μm in lower panels.

281.7 ± 45.0, 92.7 ± 51.2, and 112.9 ± 4.1 pg/brain, respectively. The amounts of PGD_2, PGE_2, and $PGF_{2\alpha}$ were greatly increased (10- to 20-fold) 2 hr after onset of SD induction (n = 5 animals; Fig. 4). Rose Bengal without photoirradiation did not affect the level of PGs (n = 5 animals).

Selective COX-2 Inhibitor Completely Arrested the Neural Activity-Dependent NREM Sleep

To verify that neuronal COX-2 up-regulated by SD is involved in such NREM sleep induction, NS-398, a selective COX-2 inhibitor, was used to suppress COX-2 activity. One hour before photooxidation for induction of SD, NS-398 (5 mg/kg, n = 5 animals) or vehicle (n = 5 animals) was intraperitoneally injected. In animals pretreated with vehicle, the amount of NREM

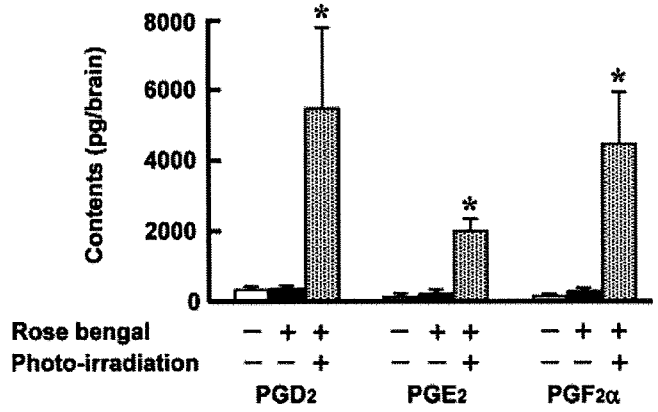

Fig. 4. Increased contents of PGD_2, PGE_2, and $PGF_{2\alpha}$ only in the cortical spreading depression (SD)-induced brain 2 hr after onset of SD. $^*P < 0.05$, two-tailed unpaired t-test.

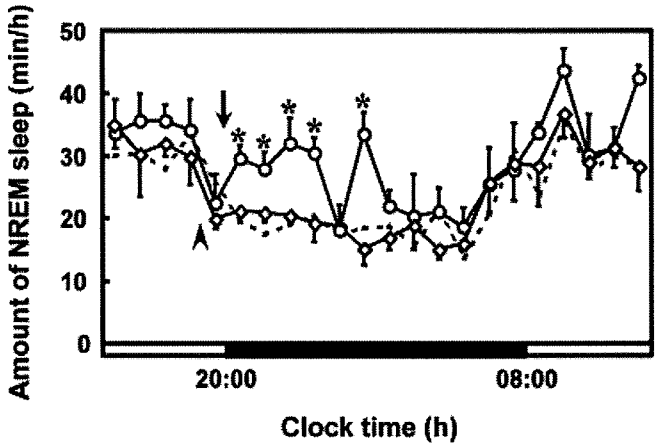

Fig. 5. NS-398, a selective COX-2 inhibitor, eliminated the cortical spreading depression (SD)-induced increment in NREM sleep. Hourly changes of amount of NREM sleep in animals pretreated with NS-398 (diamonds, n = 5) or pretreated with the vehicle (circles, n = 5). Arrowhead indicates the time of intraperitoneal injection of NS-398 or the vehicle; arrow indicates the time of SD induction in both animal groups; dashed line indicates amount of NREM sleep in the sham-operated animals that did not undergo SD induction. $^*P < 0.05$, two-way ANOVA, Scheffe's multiple-comparison procedure.

sleep was significantly increased for 5 or 6 hr after photooxidation for 30 min ($P < 0.05$, two-way ANOVA, Scheffe's multiple-comparison procedure), which was longer than the photooxidation period (10 min) used to induce NREM sleep (3 hr increase; Fig. 5). On the other hand, in the animals pretreated with NS-398, the increment of NREM sleep after SD induction was completely abrogated (Fig. 5). NS-398 itself affected neither the number of induced SD nor the behavioral states of the animals (data not shown). These results indicate that the neuronal COX-2 regulates NREM sleep stemming from aberrant brain excitation but not sleep based on circadian rhythms.

DISCUSSION

In the present study, we first demonstrated that dramatically up-regulated neuronal COX-2 expression in the cerebral cortex after aberrant brain activity is involved in the induction of NREM sleep via triggering the production of PGs. We show here that 1) COX-2 immunoreactivity was dramatically increased only in neurons of the cerebral cortex that underwent SD; 2) the amount of NREM sleep but not of REM sleep increased in those animals and the increase lasted for several hours; 3) the contents of PGs were significantly increased in brain tissue; and 4) a selective COX-2 inhibitor, NS-398, prevented the NREM sleep increase.

COX-2 was initially characterized as an inducible enzyme that is expressed in response to inflammatory stimuli, cytokines, and mitogens in nonneuronal tissues (Yermakova and O'Banion, 2000; Schwab and Schluesener, 2003). In the central nervous system, COX-2 is now known to be constitutively expressed in restricted population of neurons, including cerebral cortex and hippocampus, and its expression is up-regulated by neural activity such as synaptic activity or membrane depolarization accompanied by Ca^{2+} loading in cells (Koistinaho and Chan, 2000; Yermakova and O'Banion, 2000). Neuronal COX-2 expression was dramatically increased in variety of neurological disorders such as epilepsy, migraine and trauma, which are accompanied by aberrant brain excitation (Yamagata et al., 1993; Nogawa et al., 1997; Strauss et al., 2000). Previously, up-regulation of neuronal COX-2 expression in the brain was also observed after SD (Caggiano et al., 1996; Miettinen et al., 1997). We found here that, consistently with these reports, neuronal COX-2 expression was dramatically increased in cerebral hemisphere following SD.

COX-2 is a rate-limiting enzyme of the arachidonic acid cascade responsible for the production of PGs. To investigate the possible pathway of PGs production catalyzed by neuronal COX-2, we also examined one kind of PG synthase, L-PGDS. L-PGDS immunoreactivity is widely distributed in the leptomeninges, choroid plexuses, and parenchymal oligodendrocytes, as previously reported (Beuckmann et al., 2000). Double-immunostaining study showed that many L-PGDS-immunopositive oligodendrocytes abut COX-2-immunopositive neurons, especially in cortical layers IV–VI in the SD-induced cerebral cortex (Fig. 6A). L-PGDS immunoreactivity, however, was not different between hemispheres 2 hr after onset of SD, indicating that expression of L-PGDS was not affected by SD (Fig. 6B). L-PGDS (a member of the lipocalin superfamily; Nagata et al., 1991) is secreted by oligodendrocytes and leptomeningeal cells into the extracellular space (Beuckmann et al., 2000). In addition, Yamagata et al. (1993) hypothesized that PGH_2 is highly lipid soluble and could

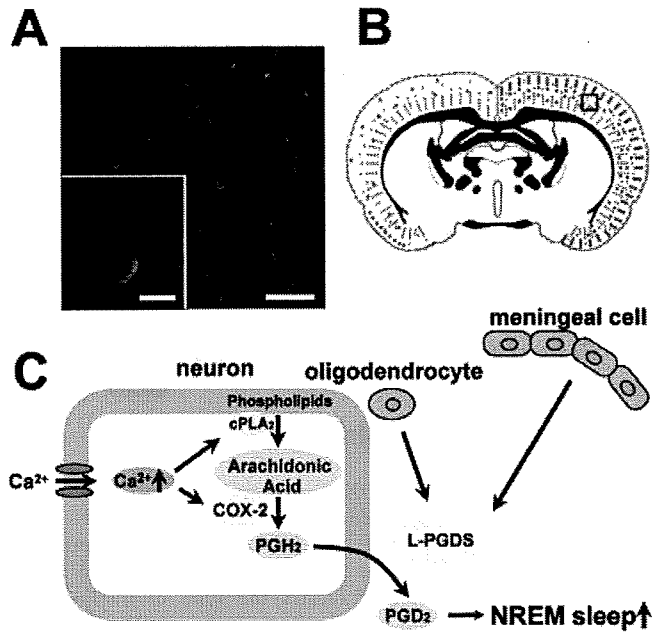

Fig. 6. Hypothetical role of the arachidonic acid cascade in increasing the amount of NREM sleep following excitation of cortical neurons. **A:** Confocal laser microscope images of immunohistochemically demonstrated COX-2 (red) and lipocalin-type prostaglandin D synthase (L-PGDS; green) in the area indicated by a rectangle in B. The **inset** clearly shows an L-PGDS-immunopositive cell abutting on a COX-2-immunopositive neuron. **B:** Drawing showing the localizations of COX-2 (red) and L-PGDS (green) 2 hr after onset of SD (the SD-induced side, right). **C:** Schema of the hypothetical mechanism of neuronal COX-2-induced NREM sleep following cortical neural activity. Scale bars = 50 μm in A; 10 μm in inset.

diffuse to the extracellular space or adjacent cells. These observations indicate that secreted L-PGDS from the leptomeninges or oligodendrocytes can convert PGH_2 produced by neuronal COX-2 into PGD_2 in the parenchymal extracellular matrix. Thus, induction of neuronal COX-2 by SD contributes at the very least to the rise in PGD_2.

PGs in the brain are known to possess sleep-promoting effects. Hayaishi and his coworkers demonstrated that content of PGD_2 in the cerebrospinal fluid of rats exhibited a circadian variation (Pandey et al., 1995) and that infusion of PGD_2 into the third ventricle or the subarachnoid space in the rostral basal forebrain induced NREM sleep in rats (Matsumura et al., 1994). After SD, PGH_2 produced by neuronal COX-2 likely increased the PGD_2 concentration in the cerebrospinal fluid and activated the sleep-promoting mechanism, as hypothesized by Hayaishi and colleagues (Fig. 6C; Hayaishi, 1988; Hayaishi and Urade, 2002). PGE_2 and $PGF_{2\alpha}$ were also reported to promote NREM sleep in rats when they were infused into the subarachnoid space in the rostral basal forebrain (Ram et al., 1997). Indeed, it has been reported that the amount of PGs dramatically increases (Forstermann et al., 1984; Parantainen et al., 1985) in disorders involving aberrant excitation of neurons, such as epilepsy and migraine, and such disorders often induce sleepiness or sleep (Sand, 1991; Donnet and Bartolomei, 1997; Kotagal, 2001; Foldvary, 2002). These reports also support our finding that SD-induced neuronal COX-2 is involved in NREM sleep via production of these PGs.

The level of COX-2 mRNA has been reported to rise within 30 min of pathological stimuli, such as seizure discharges (Yamagata et al., 1993; Chen et al., 1995), and COX-2 protein to appear 1 hr after seizure activity, peak at 3–4 hr, and remain elevated for 8 hr (Yamagata et al., 1993). Additionally, the content of PGs in the brain has been reported to increase even more rapidly after seizure, the increase in PGD_2 content being approximately 50-fold within 5 min after seizure (Forstermann et al., 1984). We found that, as reported elsewhere (Yamagata et al., 1993; Breder et al., 1995; Caggiano et al., 1996), constitutive expression of neuronal COX-2 is sporadic in the cerebral cortex, even under physiological conditions (Figs. 3, 6B). Thus, the production of PGs in the early phase (less than 1 hr) likely is due to the constitutive expression of COX-2. In the present study, the amount of NREM sleep was significantly increased also within 1 hr after onset of SD. NREM sleep induction in such an early phase following SD is thought to be due to the constitutive expression of COX-2. Because COX-2 is rapidly inactivated following conversion of arachidonic acid to PGs (Hemler and Lands, 1980), expression of the enzyme would have to be both rapid and continuous for hours to increase the amount of NREM sleep. Such a continuous expression of COX-2 in neurons for several hours was histologically confirmed in other SD-induced animals (data not shown).

COX-2 in the brain is known to be involved in NREM sleep induction following several proinflammatory cytokines treatment. NS-398, a selective COX-2 inhibitor, suppresses NREM sleep and fever induced by centrally injected proinflammatory cytokines, including interleukin (IL)-1β or tumor necrosis factor (TNF)-α (Terao et al., 1998a,b; Yoshida et al., 2003). Studies on localization of COX-2 revealed that COX-2 was expressed in endothelial cells in response to such proinflammatory cytokines centrally administrated and contributed to fever evoking (Matsumura et al., 1998; Cao et al., 2001). These observations suggest that the proinflammatory cytokine-induced NREM sleep is due to endothelial COX-2 expression in the brain. In the present study, we induced dramatic expression of COX-2 only in the cortical neurons and obtained evidence that neuronal COX-2 is involved in NREM sleep induction in response to the aberrant neural excitation in the cerebral cortex. In conclusion, we provide here a new line of evidence that neuronal COX-2 is dramatically increased in the cerebral hemisphere following cortical SD and is engaged in signal regulation of NREM sleep induction via subsequent production of PGs.

REFERENCES

Back T, Kohno K, Hossmann KA. 1994. Cortical negative DC deflections following middle cerebral artery occlusion and KCl-induced spreading depression: effect on blood flow, tissue oxygenation, and electroencephalogram. J Cereb Blood Flow Metab 14:12–19.

Beuckmann CT, Lazarus M, Gerashchenko D, Mizoguchi A, Nomura S, Mohri I, Uesugi A, Kaneko T, Mizuno N, Hayaishi O, Urade Y. 2000. Cellular localization of lipocalin-type prostaglandin D synthase (beta-trace) in the central nervous system of the adult rat. J Comp Neurol 428:62–78.

Breder CD, Dewitt D, Kraig RP. 1995. Characterization of inducible cyclooxygenase in rat brain. J Comp Neurol 355:296–315.

Caggiano AO, Breder CD, Kraig RP. 1996. Long-term elevation of cyclooxygenase-2, but not lipoxygenase, in regions synaptically distant from spreading depression. J Comp Neurol 376:447–462.

Cao C, Matsumura K, Shirakawa N, Maeda M, Jikihara I, Kobayashi S, Watanabe Y. 2001. Pyrogenic cytokines injected into the rat cerebral ventricle induce cyclooxygenase-2 in brain endothelial cells and also up-regulate their receptors. Eur J Neurosci 13:1781–1790.

Chen J, Marsh T, Zhang JS, Graham SH. 1995. Expression of cyclooxygenase 2 in rat brain following kainate treatment. Neuroreport 6:245–248.

Cui Y, Kataoka Y, Li QH, Yokoyama C, Yamagata A, Mochizuki-Oda N, Watanabe J, Yamada H, Watanabe Y. 2003. Targeted tissue oxidation in the cerebral cortex induces local prolonged depolarization and cortical spreading depression in the rat brain. Biochem Biophys Res Commun 300:631–636.

Donnet A, Bartolomei F. 1997. Migraine with visual aura and photosensitive epileptic seizures. Epilepsia 38:1032–1034.

Fabricius M, Akgoren N, Lauritzen M. 1995. Arginine-nitric oxide pathway and cerebrovascular regulation in cortical spreading depression. Am J Physiol 269:H23–H29.

Foldvary N. 2002. Sleep and epilepsy. Curr Treat Options Neurol 4: 129–135.

Forstermann U, Seregi A, Hertting G. 1984. Anticonvulsive effects of endogenous prostaglandins formed in brain of spontaneously convulsing gerbils. Prostaglandins 27:913–923.

Gerashchenko D, Okano Y, Urade Y, Inoue S, Hayaishi O. 2000. Strong rebound of wakefulness follows prostaglandin D2- or adenosine A2a receptor agonist-induced sleep. J Sleep Res 9:81–87.

Gold L, Back T, Arnold G, Dreier J, Einhaupl KM, Reuter U, Dirnagl U. 1998. Cortical spreading depression-associated hyperemia in rats: involvement of serotonin. Brain Res 783:188–193.

Gorji A. 2001. Spreading depression: a review of the clinical relevance. Brain Res Brain Res Rev 38:33–60.

Hansen AJ, Zeuthen T. 1981. Extracellular ion concentrations during spreading depression and ischemia in the rat brain cortex. Acta Physiol Scand 113:437–445.

Hayaishi O. 1988. Sleep-wake regulation by prostaglandins D2 and E2. J Biol Chem 263:14593–14596.

Hayaishi O, Urade Y. 2002. Prostaglandin D2 in sleep-wake regulation: recent progress and perspectives. Neuroscientist 8:12–15.

Hemler ME, Lands WE. 1980. Evidence for a peroxide-initiated free radical mechanism of prostaglandin biosynthesis. J Biol Chem 255:6253–6261.

Huang ZL, Qu WM, Li WD, Mochizuki T, Eguchi N, Watanabe T, Urade Y, Hayaishi O. 2001. Arousal effect of orexin A depends on activation of the histaminergic system. Proc Natl Acad Sci U S A 98:9965–9970.

Kataoka Y, Morii H, Imamura K, Cui Y, Kobayashi M, Watanabe Y. 2000. Control of neurotransmission, behaviour and development, by photodynamic manipulation of tissue redox state of brain targets. Eur J Neurosci 12:4417–4423.

Kimura H, Okamoto K, Sakai Y. 1985. Modulatory effects of prostaglandin D2, E2 and F2 alpha on the postsynaptic actions of inhibitory and excitatory amino acids in cerebellar Purkinje cell dendrites in vitro. Brain Res 330:235–244.

Koistinaho J, Chan PH. 2000. Spreading depression-induced cyclooxygenase-2 expression in the cortex. Neurochem Res 25:645–651.

Kotagal P. 2001. The relationship between sleep and epilepsy. Semin Pediatr Neurol 8:241–250.

Lauritzen M, Jorgensen MB, Diemer NH, Gjedde A, Hansen AJ. 1982. Persistent oligemia of rat cerebral cortex in the wake of spreading depression. Ann Neurol 12:469–474.

Leao AAP. 1944. Spreading depression of activity in the cerebral cortex. J Neurophysiol 7:359–390.

Matsumura H, Nakajima T, Osaka T, Satoh S, Kawase K, Kubo E, Kantha SS, Kasahara K, Hayaishi O. 1994. Prostaglandin D2-sensitive, sleep-promoting zone defined in the ventral surface of the rostral basal forebrain. Proc Natl Acad Sci U S A 91:11998–12002.

Matsumura K, Cao C, Ozaki M, Morii H, Nakadate K, Watanabe Y. 1998. Brain endothelial cells express cyclooxygenase-2 during lipopolysaccharide-induced fever: light and electron microscopic immunocytochemical studies. J Neurosci 18:6279–6289.

Miettinen S, Fusco FR, Yrjanheikki J, Keinanen R, Hirvonen T, Roivainen R, Narhi M, Hokfelt T, Koistinaho J. 1997. Spreading depression and focal brain ischemia induce cyclooxygenase-2 in cortical neurons through N-methyl-D-aspartic acid-receptors and phospholipase A2. Proc Natl Acad Sci U S A 94:6500–6505.

Nagata A, Suzuki Y, Igarashi M, Eguchi N, Toh H, Urade Y, Hayaishi O. 1991. Human brain prostaglandin D synthase has been evolutionarily differentiated from lipophilic-ligand carrier proteins. Proc Natl Acad Sci U S A 88:4020–4024.

Nedergaard M, Hansen AJ. 1988. Spreading depression is not associated with neuronal injury in the normal brain. Brain Res 449:395–398.

Nogawa S, Zhang F, Ross ME, Iadecola C. 1997. Cyclo-oxygenase-2 gene expression in neurons contributes to ischemic brain damage. J Neurosci 17:2746–2755.

Ojeda SR, Negro-Vilar A, McCann SM. 1982. Evidence for involvement of alpha-adrenergic receptors in norepinephrine-induced prostaglandin E2 and luteinizing hormone-releasing hormone release from the median eminence. Endocrinology 110:409–412.

Pandey HP, Ram A, Matsumura H, Hayaishi O. 1995. Concentration of prostaglandin D2 in cerebrospinal fluid exhibits a circadian alteration in conscious rats. Biochem Mol Biol Int 37:431–437.

Parantainen J, Vapaatalo H, Hokkanen E. 1985. Relevance of prostaglandins in migraine. Cephalalgia 5(Suppl 2):93–97.

Ram A, Pandey HP, Matsumura H, Kasahara-Orita K, Nakajima T, Takahata R, Satoh S, Terao A, Hayaishi O. 1997. CSF levels of prostaglandins, especially the level of prostaglandin D2, are correlated with increasing propensity toward sleep in rats. Brain Res 751:81–89.

Sand T. 1991. EEG in migraine: a review of the literature. Funct Neurol 6:7–22.

Schwab JM, Schluesener HJ. 2003. Cyclooxygenases and central nervous system inflammation: conceptual neglect of cyclooxygenase 1. Arch Neurol 60:630–632.

Shimizu K, Veltkamp R, Busija DW. 2000. Characteristics of induced spreading depression after transient focal ischemia in the rat. Brain Res 861:316–324.

Shinohara M, Dollinger B, Brown G, Rapoport S, Sokoloff L. 1979. Cerebral glucose utilization: local changes during and after recovery from spreading cortical depression. Science 203:188–190.

Strauss KI, Barbe MF, Marshall RM, Raghupathi R, Mehta S, Narayan RK. 2000. Prolonged cyclooxygenase-2 induction in neurons and glia following traumatic brain injury in the rat. J Neurotrauma 17:695–711.

Terao A, Matsumura H, Saito M. 1998a. Interleukin-1 induces slow-wave sleep at the prostaglandin D2-sensitive sleep-promoting zone in the rat brain. J Neurosci 18:6599–6607.

Terao A, Matsumura H, Yoneda H, Saito M. 1998b. Enhancement of slow-wave sleep by tumor necrosis factor-alpha is mediated by cyclooxygenase-2 in rats. Neuroreport 9:3791–3796.

Tobler I, Deboer T, Fischer M. 1997. Sleep and sleep regulation in normal and prion protein-deficient mice. J Neurosci 17:1869–1879.

Ueno R, Narumiya S, Ogorochi T, Nakayama T, Ishikawa Y, Hayaishi O. 1982. Role of prostaglandin D2 in the hypothermia of rats caused by bacterial lipopolysaccharide. Proc Natl Acad Sci U S A 79:6093–6097.

Yamagata K, Andreasson KI, Kaufmann WE, Barnes CA, Worley PF. 1993. Expression of a mitogen-inducible cyclooxygenase in brain neurons: regulation by synaptic activity and glucocorticoids. Neuron 11:371–386.

Yermakova A, O'Banion MK. 2000. Cyclooxygenases in the central nervous system: implications for treatment of neurological disorders. Curr Pharm Des 6:1755–1776.

Yoshida H, Kubota T, Krueger JM. 2003. A cyclooxygenase-2 inhibitor attenuates spontaneous and TNF-alpha-induced non-rapid eye movement sleep in rabbits. Am J Physiol Regul Integr Comp Physiol 285:R99–R109 [E-pub 2003 Mar].

Radiochim. Acta 96, 323–326 (2008) / DOI 10.1524/ract.2008.1498

Development of an electrochemistry apparatus for the heaviest elements

By A. Toyoshima[1,*], Y. Kasamatsu[1], Y. Kitatsuji[2], K. Tsukada[1], H. Haba[3], A. Shinohara[4] and Y. Nagame[1]

[1] Advanced Science Research Center, Japan Atomic Energy Agency, Tokai, Ibaraki 319-1195, Japan
[2] Nuclear Science and Engineering Directorate, Japan Atomic Energy Agency, Tokai, Ibaraki 319-1195, Japan
[3] Nishina Center for Accelerator Based Science, RIKEN, Wako, Saitama 351-0198, Japan
[4] Department of Chemistry, Osaka University, Toyonaka, Osaka 560-0043, Japan

(Received October 12, 2007; accepted in revised form November 21, 2007)

Electrochemistry / Flow electrolytic cell / Chemically modified electrode / Redox reaction

Summary. We developed a new apparatus for the study of electrochemical properties of the heaviest elements. The apparatus is based on a flow electrolytic cell combined with column chromatography. Glassy-carbon fibers modified with Nafion perfluorinated cation-exchange resin are used as a working electrode as well as a cation-exchanger. The elution behavior of ^{139}Ce with the number of 10^{10} atoms in 0.1 M ammonium α-hydroxyisobutyric acid solution from the column electrode was investigated at the applied potentials of 0.2–1.0 V versus the Ag/AgCl reference electrode in 1.0 M LiCl. It was found that $^{139}Ce^{3+}$ is successfully oxidized to $^{139}Ce^{4+}$ even with tracer concentration at around the redox potential determined by cyclic voltammetry for the macro amounts of Ce with 10^{17} atoms (10^{-3} M). The present oxidation reaction and separation of Ce^{4+} was accomplished within a few minutes.

1. Introduction

The heaviest atoms with atomic numbers ≥ 101 must be produced in heavy-ion-induced nuclear reactions. Because of the short half-lives and the low production rates, chemical experiments are carried out on an atom-at-at-time basis. According to the concept of single-atom chemistry by Guillaumont *et al.* [1, 2], it is suggested that an equilibrium constant of the atom between two phases is correctly determined in terms of the probability of finding the atoms in one phase or the other. Thus, currently favorable experimental techniques for the chemical study of the heaviest elements are based on partition methods such as ion-exchange chromatography, solvent extraction, and gas chromatography [3, 4].

Oxidation-reduction (redox) studies of the heaviest elements are expected to give valuable information on valence electron states such as oxidation states and redox potentials. Ordinary electrochemical approaches such as cyclic voltammetry are, however, not available for the single-atom chemistry of the heaviest elements. Thus, one needs to investigate redox properties of the heaviest elements based on partition behavior of the single atoms between two phases instead of measurement of electric currents arising from a redox reaction.

Radiochemical polarography has been applied to the determination of the amalgamation potentials of element 101 (mendelevium, Md) [5] and element 102 (nobelium, No) [6, 7] where amalgamated metals were extracted into the mercury phase from aqueous solution. The amalgamation technique gives reduction potentials from the most stable oxidation states to amalgamated metallic-states.

Another technique is the column chromatography with simultaneous use of reducing and oxidizing agents, which is based on differences in adsorption abilities between ions with different oxidation states. The existence of the divalent state of Md [8–10] and the trivalent one of No [11, 12] in aqueous solutions has been verified based on the chromatographic behavior comparing with that of some indicative radiotracers. It is, however, difficult to apply this technique to the heavier elements with shorter half-lives because of the time-consuming and complicated procedures.

In the present study, we newly developed an electrochemistry apparatus to identify possible oxidation states of the heaviest elements in aqueous solutions. The apparatus is based on a flow electrolytic cell [13–15] equipped with a chemically modified electrode [16–19] that is quite suitable for rapid and efficient chemical experiments of the heaviest elements. A chemically modified method was applied to separate ions of interest in different oxidation states on the electrode. We studied the oxidation reaction of $Ce^{3+} \rightarrow Ce^{4+} + e^-$ with macro- and tracer-amounts of concentration of Ce in 0.1 M ammonium α-hydroxyisobutyric acid (α-HIB) solution by separating Ce^{3+} and Ce^{4+} in elution procedures. First, cyclic voltammetry of Ce with 10^{17} atoms (10^{-3} M) in 0.1 M α-HIB solution was performed to determine the redox potential of the $Ce^{4+} + e^- \rightleftarrows Ce^{3+}$ reaction under the present condition. Then, the elution behavior of the radiotracer ^{139}Ce with 10^{10} atoms on the chemically modified electrode was investigated at the applied potentials of 0.2–1.0 V. The applicability of the present apparatus to single-atom chemistry is demonstrated.

*Author for correspondence
(E-mail: toyoshima.atsushi@jaea.go.jp).